

# **Highest bias stability fiber-optic gyroscope SRS-5000**

**Yu.N.Korkishko, V.A.Fedorov, V.E.Prilutskiy, V.G.Ponomarev, I.V.Fedorov,  
S.M.Kostritskii, I.V.Morev, D.V.Obuhovich, S.V.Prilutskiy,  
A.I.Zuev, V.K.Varnakov**

LLC RPC Optolink,  
Sosnovaya alley, building 6a, premises 5,  
124489, Zelenograd, Moscow  
RUSSIA

Inertial Sensors and Systems 2017  
Karlsruhe, Germany

## Abstract

The aim of the current work was to produce the highest bias stability fiber-optic gyroscope SRS-5000 and to evaluate its main technical characteristics. Five prototype SRS-5000 devices were comprehensively measured and evaluated. Measured devices' parameters (ARW around  $69 \mu^\circ/\sqrt{\text{hour}}$  with bias stability better than  $8 \times 10^{-5} \text{ }^\circ/\text{hour}$ ) allow to assess this type of devices as the highest-precision strategic grade fiber-optic gyroscopes, commercially available.

### 1. Highest bias stability fiber-optic gyroscope SRS-5000

Today the fiber-optic gyroscopes (FOGs) reach ultimate theoretical performance and surpass well-established competitor, the ring laser gyroscopes [1-3]. Due to its inherent low random noise and its scalability, FOG technology is one of the very few technologies able to cope with the applications requiring the highest performance. The FOG technology is seen by US experts as the only technology in the future able to replace the mechanical gyroscopes used for SSBN (Sub-Surface Ballistic Nuclear). Up to date, the highest performance FOGs are space grade FOGs - Honeywell HPFOG [4-8], AlliedSignal FOG [9], Litton FOG [10], L-3com Cirus [11], Airbus (former Astrium) Astrix-200 [12], as well as iXblue Marins [13], and iXBlue FOG-prototypes [14,15]. Parameters of up-to-date highest performance FOGs are presented in the Table 1.

**Table 1. Parameters of up-to-date highest performance FOGs**

FOG, Manufacturer	ARW, $\times 10^{-6} \text{ }^\circ/\sqrt{\text{hr}}$	Bias instability, $\times 10^{-5} \text{ }^\circ/\text{hr}$	Scale factor error, ppm	Coil length and diameter
HPFOG, Honeywell [4-8]	100	30	1	4 km
AlliedSignal Guidance and Control Systems [9]	210	57		2 km
Litton Guidance and Control Systems [10]	900	90	10	1 km, 76 mm
CIRUS-A, L-3 Space & Nav. [11]	500	300	10	
Astrix-200, Airbus Defence & Space [12]	200		30	5 km, 200 mm
Marins, Ixblue [13]	180	10		5 km
Prototype FOG, Ixblue [14,15]	39			5 km
SRS-2000, Optolink	180	10	30	2 km, 250 mm
SRS-5000, Optolink	69	8	3	5 km, 250 mm

Research & Production Company Optolink has so far developed and produces series of single-axis FOGs SRS-2000, SRS-1000, SRS-501 and SRS-200 with different fiber coil lengths and diameters, as well as three-axis FOGs TRS-500 and inertial measurement units IMU-500, IMU-501 and IMU-1000 [16-23]. To achieve great flexibility, Optolink has developed Interferometer-FOG that follows strictly the well-known Reciprocal Configuration. In order to take all the benefits of this configuration, it is combined with an original PM fiber, a high performance Integrated Optical Circuit (IOC), and a powerful All-Digital Signal Processing. Optolink's expertise in those 3 elements allowed us to develop high performance FOGs. Detailed passive thermal design, coil winding and gyro assembly techniques, methods for rejecting light source intensity noise and light source wavelength control are critical features that have been developed to produce a FOG with low noise, stable bias, and a stable and linear scale factor. Optolink's ultimate performance FOGs are the result of more than 15 years of research and development, and they address the most demanding applications and performance from 0.1 °/hour to 0.0001 °/hour. Today Optolink directly masters and controls the full chain of key technological FOG components from the manufacturing of the fiber and integrated optical circuit to coil winding and the optical integration of components.

High-precision Optolink's FOGs SRS-1000 and SRS-2000 are successfully used by customers (with confirmation of their specified parameters) [24-31], particularly by NASA for precision pointing and attitude control of the Balloon Experimental Twin Telescope for Infrared Interferometry (BETTII) [24-27] to study galactic clustered star formation to provide spatially-resolved spectroscopy in the far infrared with attitude knowledge at a level of 2 milliarcseconds and with accurate absolute attitude determination at the half arcsecond level, as well as for first investigation of relativistic frame dragging phenomenon (Lense–Thirring effect) in Earth conditions [28-30], and for nanopositioning purposes by piezo-activated rotation table with the smallest velocity steps resolved and reported in the literature so far [31].

The bias instability of a gyro, a measure of gyro output variation when subjected to a constant input, is an important parameter for all applications. It dictates the accuracy of the navigation or the attitude reference system employing these gyros. The chief contributors to bias instability in a fiber optic gyroscope are time dependent nonreciprocities and polarization errors. Our efforts over all years were focused on configuring optical circuits with little or no residual polarization error. In addition, coil winding, fiber routing and packaging, and thermal management expertise proved to be key skills required to achieve

FOG performance. At Optolink, experience gained during the course of production of over 4000 close loop IFOGs has honed the skills of our work force and is an important reason for our success with high-precision FOGs.

Angle Random Walk (ARW) is a measure of random noise present in the gyro output. The major sources of random noise in a FOG are (in decreasing order of magnitude) backscattered light from fiber imperfections, photon shot noise in the detector, electronic thermal noise and intensity fluctuations in the light source. A light source with a very short coherence length, typically a broadband light source, minimizes the effects of fiber backscatter. Photon shot noise is caused by photons randomly impinging on the detector, and its effect decreases in proportion to the square root of the power reaching the detector. Typically all our high-precision gyros use a high powered light source, reducing the photon shot noise to a very low level. At high light source powers, fluctuation in the light source intensity becomes a dominant noise contributor - known as Relative Intensity Noise (RIN). The task of SRS-5000 production would place lots of challenges for us, mainly because of specific temperature sensitivity of long-coil gyro and also the requirement of extremely low noise electronic part. However, we succeeded and for the time being the device is in full-scale serial production. The device has PM-fiber coil length and winding radius of 5000m and 12cm, respectively. In order to correctly measure device main parameters ppm-tolerance rotation tables are to be used. Also, noise of the external environment should be as low as possible.



Figure 1a. View of SRS-5000



Figure 1b. Procedure of SRS-5000 devices testing in 2-axis motion simulator Acutronic AC2247-TCM

Figure 1. View of SRS-5000 gyro

## 2. SRS-5000 constituents and its functional scheme

The SRS-5000 device constituents are:

- Optical block with the following constituents: ring fiber-optic coil (FC); multifunctional integrated optical module (MIOM); superluminescent diode (SLD); photodiode (TFD-50MR);
- Photocurrent amplifier circuit (PAC) with photodiode (TFD-50MR);
- Circuit of phase modulation signal amplification (CPMA);
- SLD control board (SCB) at which the SLD is installed;
- Digital signal processor (DSP);
- Interface board (IB).

The device structure is presented in Figure 2.

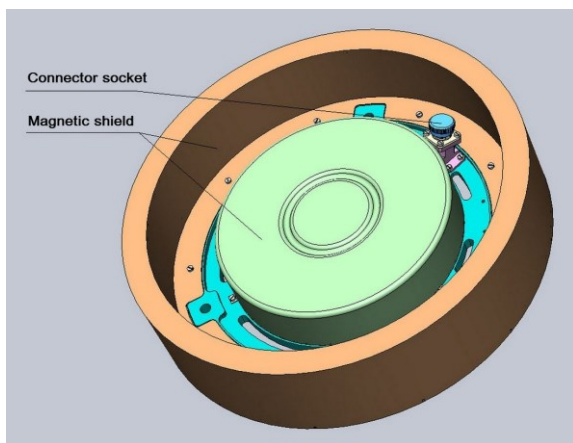


Figure 2a. View with mounted top

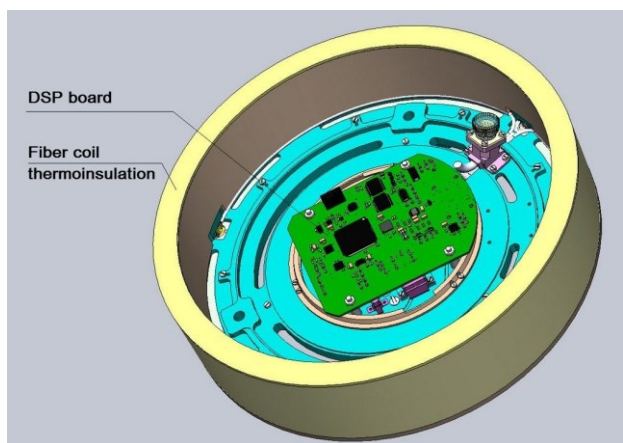


Figure 2b. DSP board view

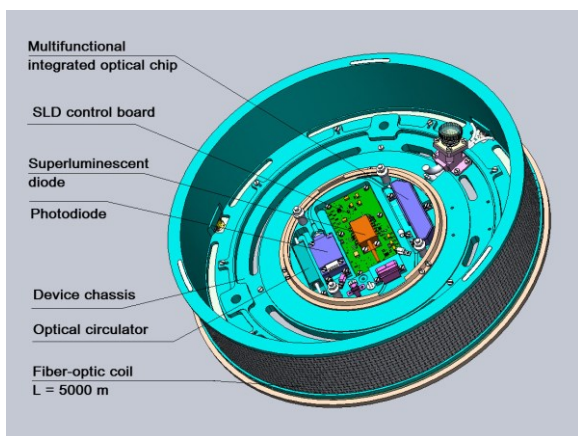


Figure 2c. Optical block view

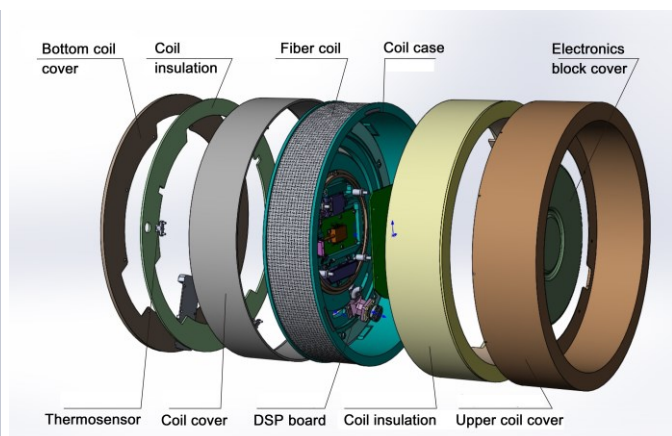


Figure 2d. Fiber-optic coil view

Figure 2. Structure of SRS-5000 gyro

Functional scheme of the device is presented in Figure 3.

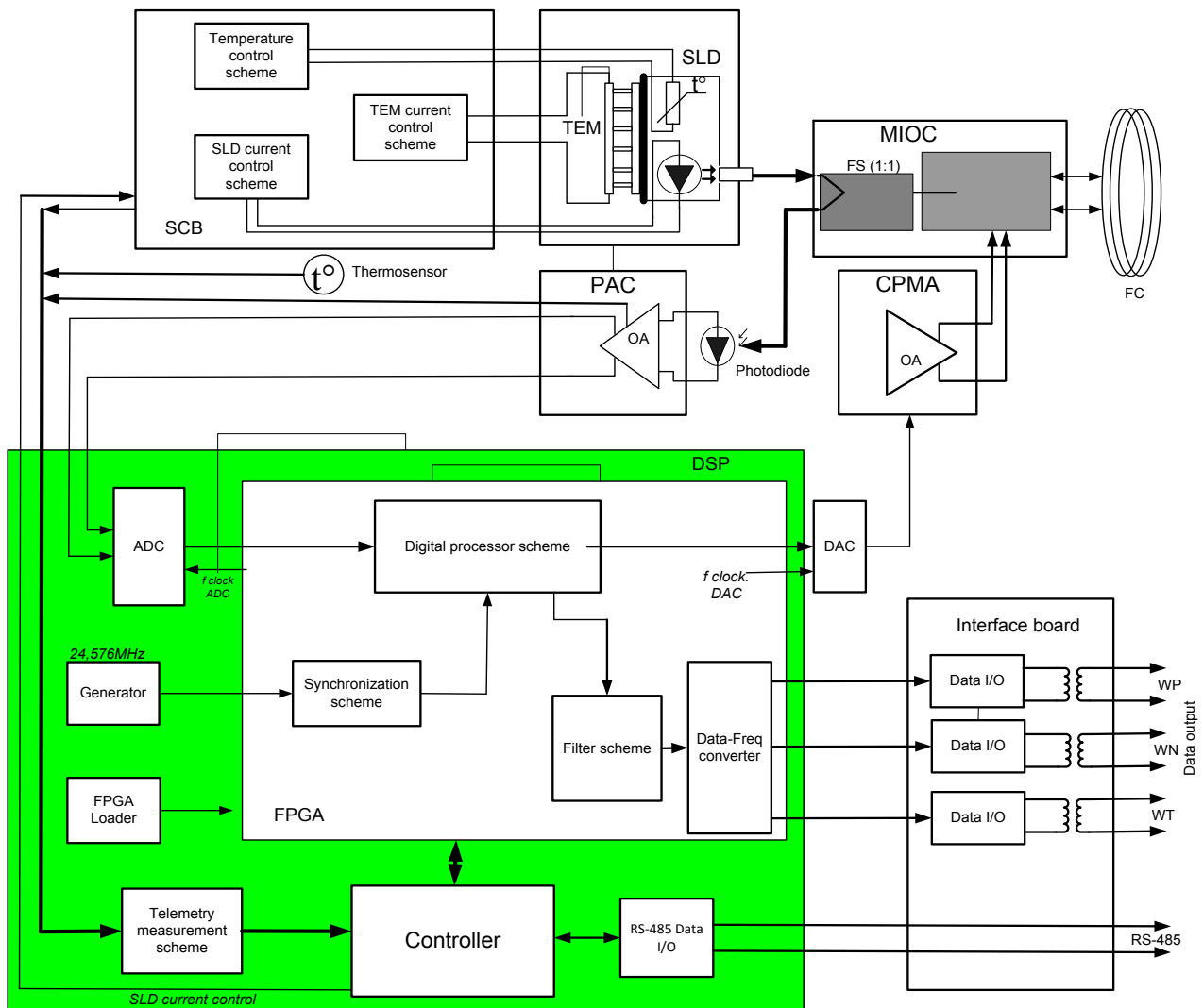


Figure 3. Functional scheme of SRS-5000 gyro

**List of used abbreviations in Figure 3**

- |   |                                       |
|---|---------------------------------------|
| MIOC - multifunctional integrated optical chip, | FS – fiber splitter,                  |
| TEM – thermoelectric module,                    | OA – operational amplifier,           |
| DAC – digital-analog converter,                 | ADC – analog-digital converter,       |
| $F_{\text{clock}}$ - clock frequency,           | FPGA – field-programmable gate array. |

### 3. SRS-5000 operation scheme and performance

The sensitive part of device optical scheme consists of the fiber-optic coil wound onto the cylindrical coil base. Fiber-optic coil is made of specially made by Optolink polarization maintaining (Panda-type) optical fiber. Fiber coil length and diameter is 5000 m and 240 mm, respectively. To reduce Shupe error, coils for FOGs are produced in a octupole pattern [32, 33] packed with glue to achieve high performance. Coil with optical fiber is places into the cylindrical base on the SRS-5000 chassis. In the inner volume of the coil all the electronic parts of the gyro are located: multifunctional integrated optical module (MIOM); superluminescent diode (SLD); photocurrent amplifier circuit (PAC) with photodiode (TFD-50MR); circuit of phase modulation signal amplification (CPMA); SLD control board (SCB); digital signal processor (DSP) and interface board (IB). Photodiode TFD-50MR and MIOM unit are produced with input/output pigtails of multi-mode and single-mode PM optical fibers of the own company production.

Optical signal that contains the angular rate data is converted to electrical signal, amplified with PAC and goes to DSP board, where the closed-loop scheme controls the phase shift between the counter-propagating lightwaves. It is known that FOG maximal bias error that comes from polarization non-reciprocity depends on fiber coil parameters and also on lightwave polarization characteristics [34]:

$$\Delta\Omega_p^{\max} \leq \frac{\lambda c p \varepsilon}{DL} \sqrt{\frac{\lambda \sqrt{\ln 2}}{\pi \Delta\lambda} h L_p},$$

where  $\lambda$  - central wavelength,  $\Delta\lambda$  - spectral width,  $P$  - degree of residual polarization of the input lightwave,  $\varepsilon$  - extinction ratio of polarizer,  $h$  - ratio of intermodal polarization coupling,  $L_p$  - length of polarization beats in FC,  $c$  - speed of light.

Spectral noise power (Angle Random Walk, ARW) derived in the result of taking into account all the main noise factors under the auxiliary modulation depth  $\frac{\pi}{2}$ , is evaluated according to the following formula [35]:

$$W = \frac{\sqrt{2} \lambda c}{2\pi DL} \sqrt{\frac{4kT}{R\eta^2 P^2} + \frac{e i_d}{\eta^2 P^2} + \frac{e}{\eta P} + \frac{\lambda^2}{4c\Delta\lambda}},$$

where  $k$  - Boltzmann's constant,  $R$  - resistance of the transimpedance transducer of the photodetector device,  $\eta$  - efficiency ratio of photodiode,  $P$  - incident lightwave power on photodiode,  $e$  - elementary charge,  $i_d$  - photodiode dark current.

The first term of the sum under the radical sign determines the thermal noise of the amplifier, the second - the noise of the dark current, the third - the shot noise and the fourth - the excessive noise of the SLD.

To achieve a minimum excess noise of the SLD, a superluminescent diode with a maximum spectral width of 100 nm was used as a light source. The control board of the emitter of the SCB, on which the SLD diode, built-in thermal sensor and TEM are installed, provides the thermal regime of the emitting SLD crystal within the limits  $(25 \pm 0.1)$  °C with the help of the TEM, and thereby stabilizes the power and wavelength of the SLD emission.

The DSP board of the device is located on the bottom side of the device chassis. The DSP board converts the analog signal from the PAC into a digital code and then converts the code into a sawtooth voltage with a slope proportional to the measured angular velocity.

The interface board has two versions. Depending on the variant, the type of output information about the measured angular velocity differs:

1. Measured angular rate data is given in the form of a bipolar signal consisting of two pulses of positive and negative polarity of a given duration and a given interval between the leading edges of the pulses. The repetition rate of a pair of pulses is proportional to the projection of the angular velocity vector onto the measuring axis of the device. The bipolar signal is transmitted via separate communication lines for different polarities of the measured angular velocity. When the device rotates in the positive direction relative to the measuring axis, a bipolar signal is formed at the contacts ("WP +", "WP-"). When the device rotates in the negative direction relative to the measuring axis, a bipolar output signal is formed at the contacts ("WN+", "WN-"). Simultaneous appearance of pulses on the outputs "WP" and "WN" is excluded.

2. Measured angular rate data is output via RS-485 interface in the form of data frames of fixed length. Angular rate measurement and corresponding data frame output is performed using an external clock. In this version of the device built-in test function is implemented, which allows the unit to evaluate the operability of the device itself.

The internal arrangement of the SRS-5000 components in the device is shown in Figure 4.



Figure 4. Internal arrangement of the SRS-5000 components in the device

The device is powered by voltage reducing transformers with galvanic isolation. The main technical characteristics of the SRS-5000 gyro are shown in Table 2.

**Table 2. Main technical characteristics of the SRS-5000 gyro**

Parameter	Value
<b>*Measurement range, °/s</b>	<b>*±12 (<u>±550</u>)</b>
**Bias Instability in single launch, °/hour	$8 \times 10^{-5}$
***Bias Drift at constant temperature, °/hour	$5 \times 10^{-4}$ ( $1\sigma$ )
**Angle Random Walk, °/√hour	$7 \times 10^{-5}$
Scale Factor (SF) error in launch, ppm	10
Power consumption, W	7
Mass, kg	1.7
Dimensions, mm	Ø250×45
Fiber-optic coil length, m	5000
Fiber-optic coil diameter, mm	240

**\*Dynamic range can be extended via scheme reported for SRS-1000 at ISS2014 [21].**

\*\*According to Allan Variance (Allan Deviation) plot.

\*\*\*Standard assessment, commonly used in Russia for bias stability parameter (however, outdated due to much larger than 100s instability time)

## 4. Measurement results

### 4.1. Bias instability tests in single launch

For first SRS-5000 produced we performed short-term stability tests that implied evaluation of a gyro bias stability in single launch at constant temperature. Allan variance plots for SRS-5000 ground tests are shown in Fig. 5 with respect to Allan variance results for the most advanced IxBlue FOGs: MARINS FOG [13], 5000m-coil FOG [14], and FOG for rotational ground motions measurement [15] with ARW = 38 and 180  $\mu^\circ/\sqrt{\text{hour}}$ , respectively. According to measurement results, the main SRS-5000 parameters are: dynamic range  $\pm 12^\circ/\text{s}$ ; angle random walk (ARW)  $< 70 \mu^\circ/\sqrt{\text{h}}$  ( $< 20 \text{ nrad} \times \text{s}^{-1}/\sqrt{\text{Hz}}$ ); bias instability (BI)  $< 8 \times 10^{-5}^\circ/\text{hour}$  with characteristic averaging time of BI shelf  $> 5000\text{s}$ ; scale factor repeatability  $\leq 3\text{ppm}$  ( $1\sigma$ ); see Table 3.

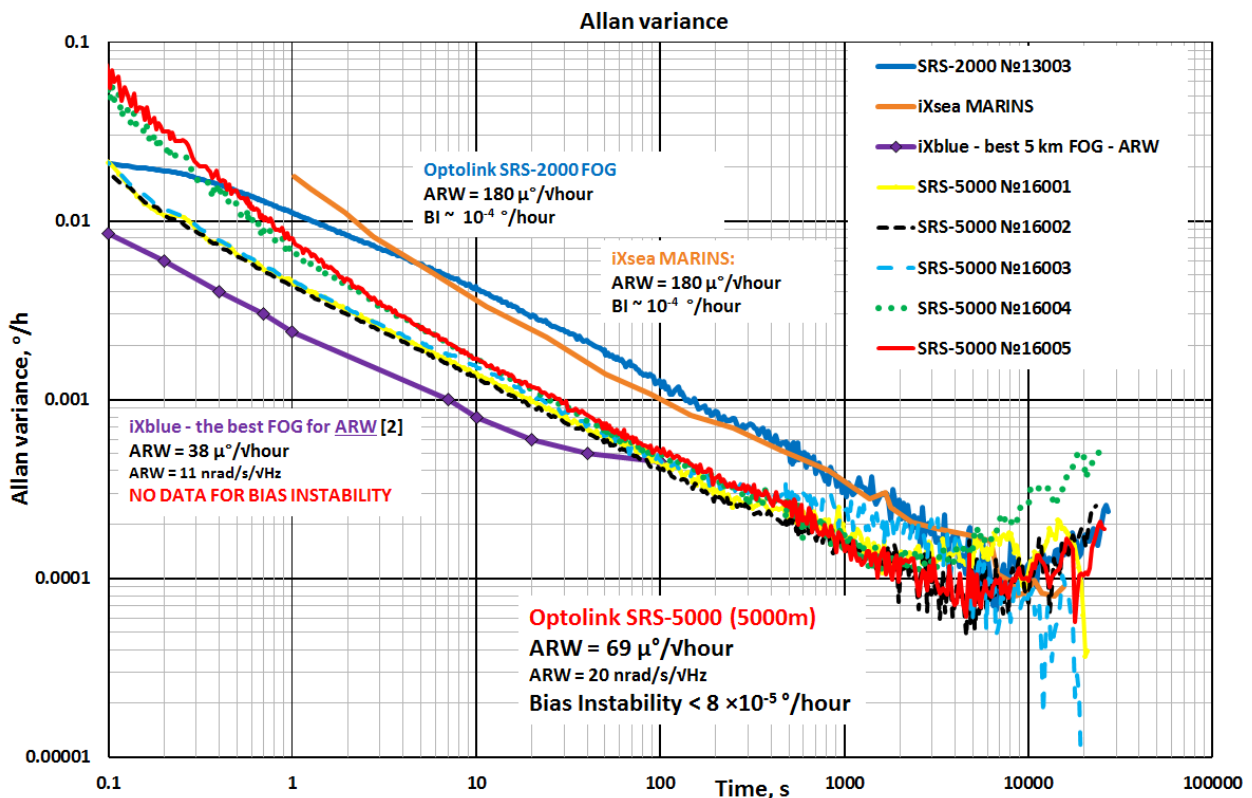


Figure 5. SRS-5000 Allan variance plot, compared with IxBlue best FOG results presented [13-15]

Best results in the sense of Allan variation plots were obtained at Optolink's facility in Saratov – the test site was vibration-isolated plate on standalone basement in the bomb shelter. The curves corresponding to these launches can be observed in Figure 5, plots for SRS-5000 №№ 16001, 16002, 16003 units. Tests for units №№ 16004, 16005 were conducted in Optolink's facility in Zelenograd, Moscow, where the environment did not permit vibration-isolated conditions. This fact explains slightly higher noise level at lower

averaging times for Zelenograd launches if compared with Saratov data. However, despite the external noise easily observed on SRS-5000 №16005 graphs of raw 400Hz-signal and its 100-second gliding average in Fig.6, bias instability shelf level is not affected.

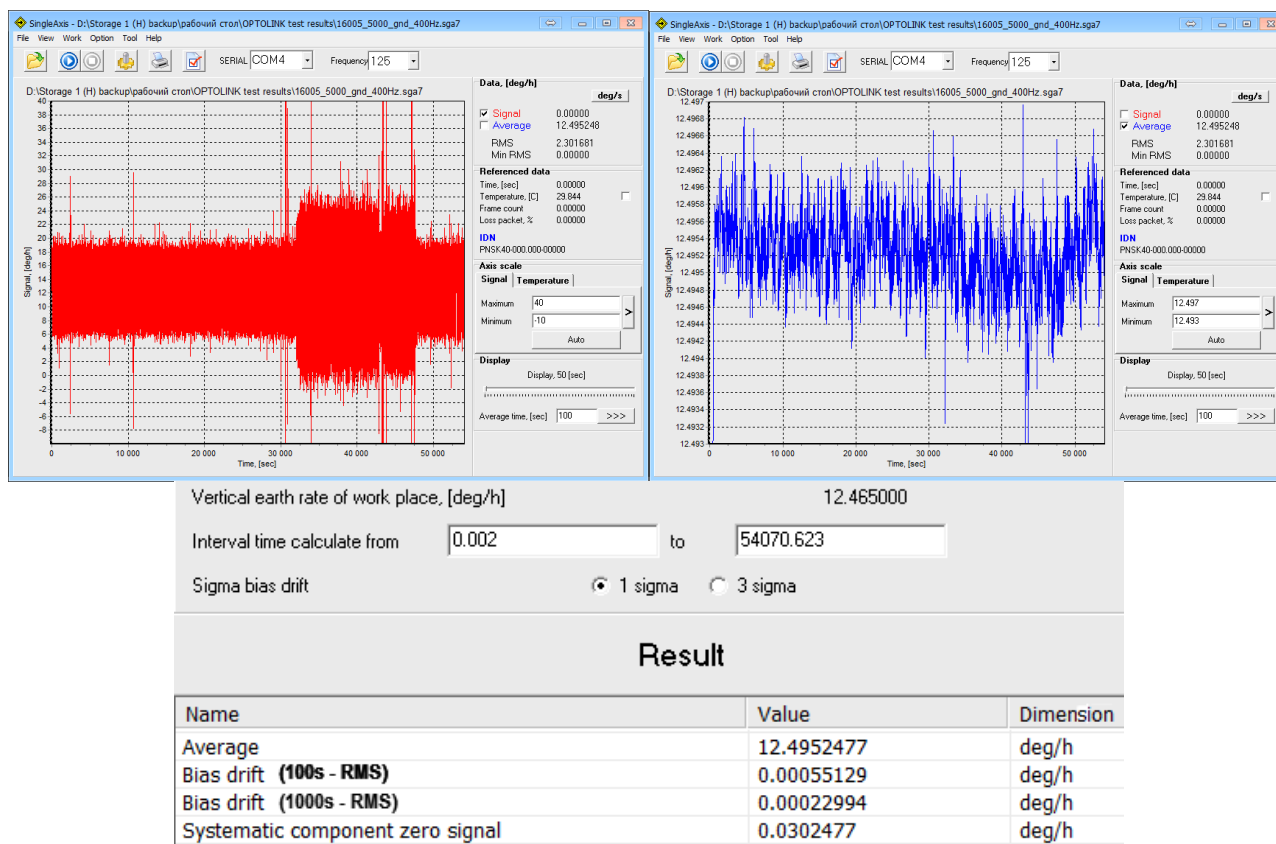


Figure 6. SRS-5000 №16005 raw signal and its 100-second gliding average, tests in Zelenograd.

Lower image shows the results of gyro parameters evaluation using this data

Starting from the device manufacturing and till the end of all measurements, no bias corrections were introduced into SRS-5000 devices, thus the device signal has certain bias error, which for SRS-5000 №16005 is 0.0302 °/hour. Bias drift (unbiased RMS of signal mean values for distinct time periods, usually 100-second intervals, the merit widely used in Russia) amounted  $5.5 \times 10^{-4}$  °/hour for 100s-averaging time and  $2.3 \times 10^{-4}$  °/hour for 1000s-averaging time, which is the best reported value for gyros produced in Russia for the time being.

From the comparison of Allan variance plots for Optolink and IxBlue FOGs we conclude that SRS-5000 can be considered the highest precision class FOG with bias instability and noise level not higher (not worse) than the best IxBlue 5000m-coil FOG and MARINS devices [13-15].

From the viewpoint of accumulated angle, for SRS-5000 devices we also estimated the Noise Equivalent Angle (NEA) parameter, which is the additional parameter of Fog performance to check. NEA peak-to-peak value represents the possible maximum value of angular error in static position (or in dynamics with respect to more accurate angle control sensor) for a definite time interval, e.g. this value is often observed and responsible for heading drift in the tasks of SINS inertial navigation. Thus it is the real measure of SINS output angle (heading, roll, pitch) stability, which is of major importance for real applications. The nature of NEA peak-to-peak error is the intrinsic gyro noise and gyro bias/SF instability (without further differentiation of the noise/instability) source, the fact that it takes into account all error sources inside makes NEA an objective and prominent assessment parameter.

We measured NEA only during static launches, due to the fact that in dynamics NEA error is mainly caused by SF error and instability (see also SF angular increment measurements, p. 4.4, Fig. 13) In static, the FOG angular rate was integrated over time with subtraction of mean angular rate to eliminate Earth rotation from the accumulated angle. As shown in Fig. 7, for time period durations of 1800s (0.5h), 3600s (1h), 16000s (4h) the peak-to-peak NEA values amounted:  $90\mu^\circ$  (0.31 arcsec),  $110\mu^\circ$  (0.37 arcsec) and  $190\mu^\circ$  (0.69 arcsec), respectively. In summary, we have obtained NEA peak-to-peak angle, and thus maximal angle drift less that  $1/5000^\circ$  over more than 4 hours of operation.

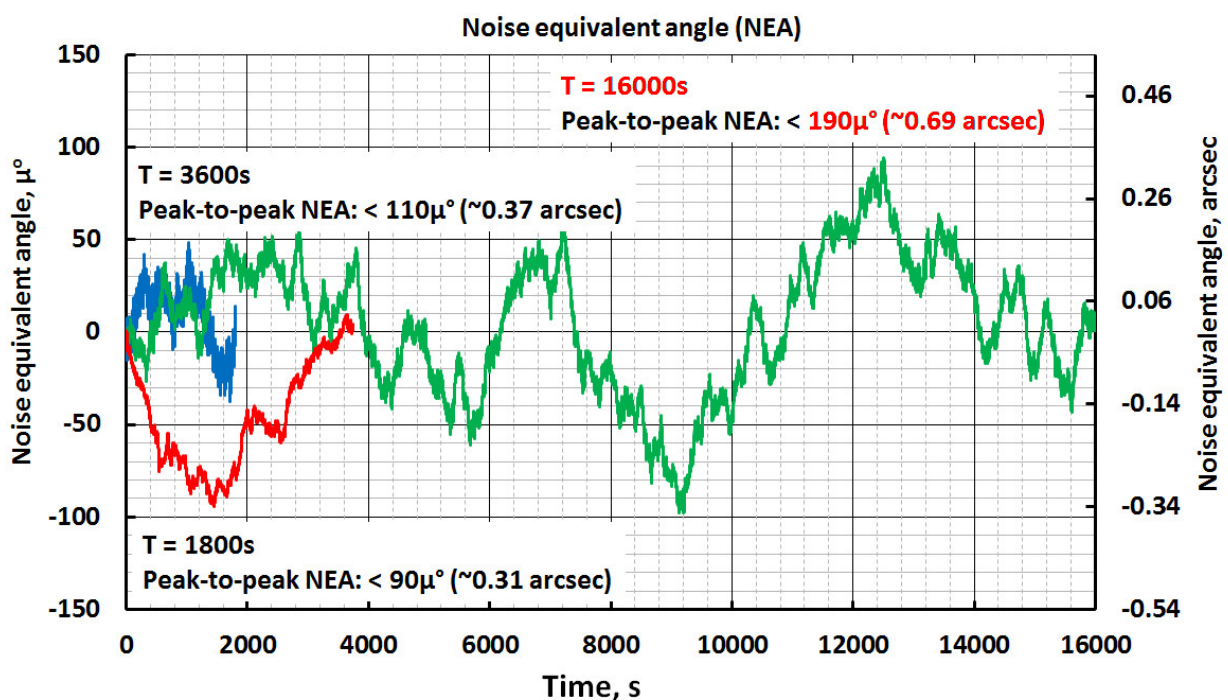


Figure 7. SRS-5000 Noise equivalent angle (NEA) estimation over time

## 4.2. Bias repeatability (run-to-run) tests and bias long-term stability results

Bias repeatability tests were also conducted. First test sequence was aimed at estimating run-to-run bias stability of SRS-5000 gyros. Before these short-term tests we waited until the temperature in the running device was stabilized, and then in the single data record repowered-on the device every 10 minutes. Period of power outage was 30 seconds. Statistics of mean values in each consequent launch in the run-to-run test can be observed in Fig. 8, launch mean values RMS value was  $6 \times 10^{-4}$  °/hour.

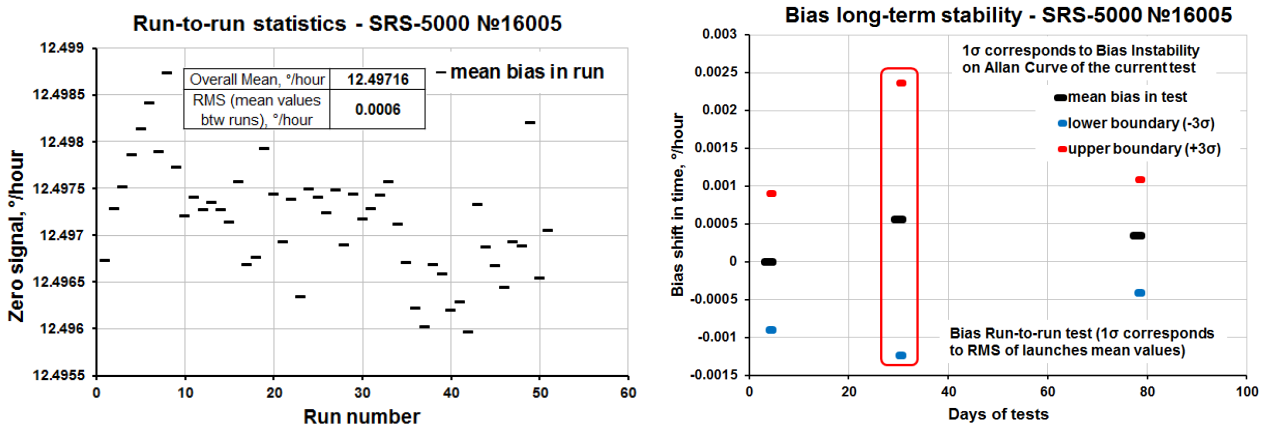


Figure 8. SRS-5000 №16005 stability tests: Left - run-to-run test; right – bias long-term stability test

Second test sequence was aimed at estimating long-term bias stability of SRS-5000 gyros, in these tests long runs of SRS-5000 gyro were repeated with the period of several weeks and eventual point of half-a-year term. Between the measurement periods generally the device was not run. During the first 3 months the bias was stable with maximal drift of  $5.6 \times 10^{-4}$  °/hour (mean of run-to-run measurements on the 30<sup>th</sup> day), thus 80-day bias instability is within range  $\pm 3 \times 10^{-4}$  °/hour, which is the best obtained result for Optolink's gyroscopes.

### 4.3. Angular rate and Angle Power spectral density (PSD) analysis

In order to examine external noise sources and intrinsic noise nature of SRS-5000 gyro signal we analysed power spectral density (PSD) of gyro signal (angular rate) and derived angle (NEA – angle PSD) in ground tests, shown in Figure 9. In Figure 9 three different measurements are shown that correspond to 70Hz sampling rate tests at Optolink’s Saratov facility (isolated basement in bomb shelter), 400Hz and even 8kHz sampling rate tests at Optolink’s Zelenograd facility (1<sup>st</sup> floor, no vibration isolation or dampening).

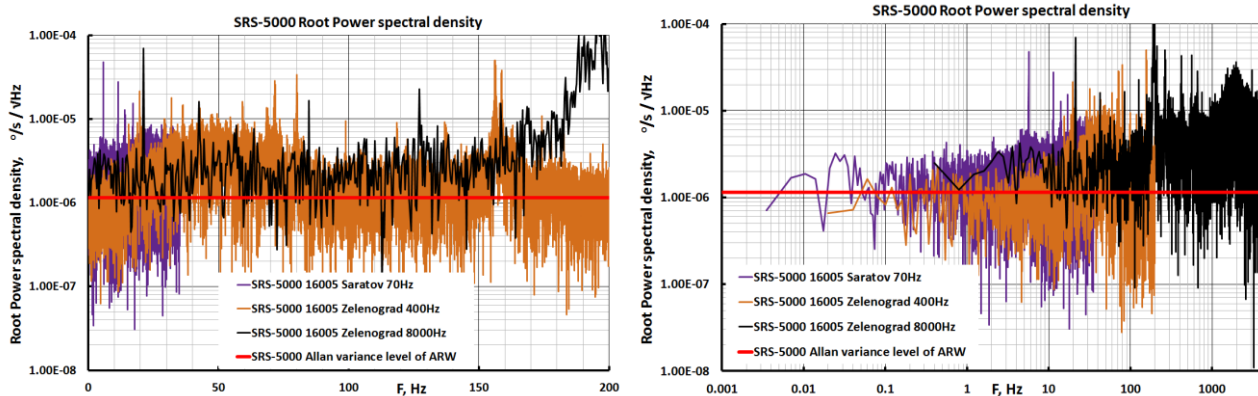


Figure 9. Power spectral density of SRS-5000 №16005 signal, 70Hz Saratov test, 400Hz and 8kHz Zelenograd tests: left – semi-logarithmic plot, right – logarithmic plot. Red line corresponds to ARW value of  $1.15 \mu^\circ/\text{s}/\sqrt{\text{Hz}}$  obtained from Allan Variance plots.

70Hz and 400Hz tests show nearly the same mean value of PSD that equals ARW data from Allan variance plot ( $1.15 \mu^\circ/\text{s}/\sqrt{\text{Hz}}$ ,  $69 \mu^\circ/\sqrt{\text{hour}}$ ), and the shape of curve is close to white noise, without serious disturbances in 200Hz-frequency range. Range of 20-80 Hz is somewhat higher than overall value, the nature is considered intrinsic due to large bandwidth (disturbance peaks are rather sharp). For 8000Hz-sampling rate, we were able to obtain PSD graphs up to Nyquist frequency of 4000Hz: a little higher ARW value is observed ( $1.83 \mu^\circ/\text{s}/\sqrt{\text{Hz}}$ ), however even up to 4000Hz the band is straight (white noise nature) due to the absence of internal improving filters in SRS-5000 in all tests.

In addition, we analysed Angle PSD to indicate the level of Angle White Noise (AWN), usually used as a tolerance parameter for high-performance gyroscopes. For angle derived in terms of NEA, Angle PSD is presented in Fig. 10. It can be seen that all the plots are in strict agreement with ideal angle PSD curve obtained from Allan Variance ARW level value, and what is more important, there is no AWN shelf and angle quantization observed: down to the level of  $10^{-6} \text{ arcsec}/\sqrt{\text{Hz}}$ . This fact unambiguously indicates ideal mastering of all noise types in SRS-5000 gyro.

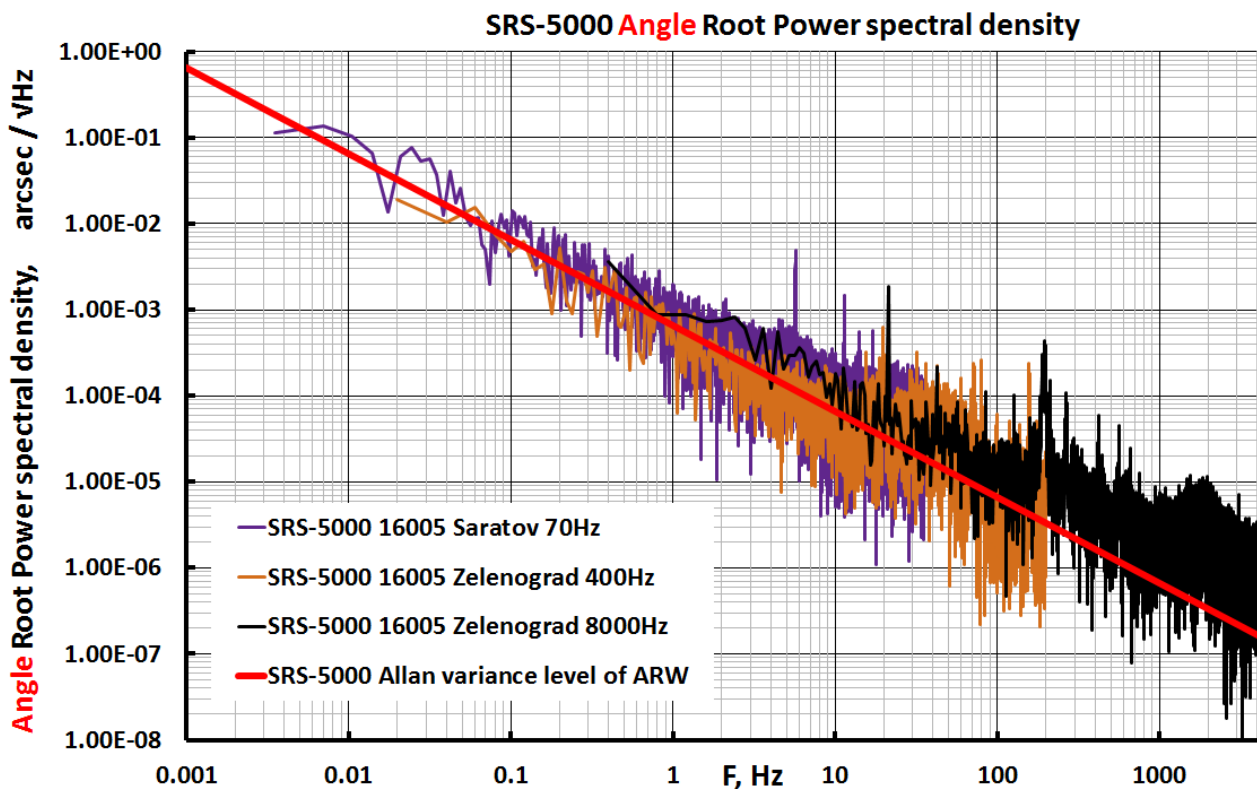


Figure 10. **Angle** Power spectral density of SRS-5000 №16005 signal, 70Hz Saratov test, 400Hz and 8kHz Zelenograd tests. Red line corresponds to ARW value of  $1.15 \mu^\circ/\text{s}/\sqrt{\text{Hz}}$  obtained from Allan Variance plots. **No Awn shelf observed** down to the level of  $10^{-6}$  arcsec/ $\sqrt{\text{Hz}}$ .

#### 4.4. Scale factor stability tests

Scale factor (SF) stability also was investigated. Initial temperature scale factor compensation was introduced during the production at our facility in Saratov, but during all the tests it remained unchanged. As the SF in temperature range even despite the initial compensation little but differs, all the SF measurements were conducted in temperature chamber with horizontal plane single-axis rotation table at constant temperature, namely  $30^\circ\text{C}$ . Temperature point was not specifically chosen, but was convenient as the bias stability measurements also proceeded near this temperature point, and the temperature chamber's power load was not too high and excessive. Test procedure consisted of a periodic sequence of turn at defined rotation rates: 6, 8, 10, 12  $^\circ/\text{s}$  and both rotation directions. For some tests 4  $^\circ/\text{s}$  or slower rates were used, but it was noticed that rotation table's servo did not perform equally well and the rotation rate consequently had higher dispersion that spoiled the measurements. Figure 11 shows the raw data record of SF stability measurements. Each dot in the graphs represents the error of single rotation, evaluated using the desired rotation rate of table and the vertical earth rotation rare projection. It is necessary to mention that the mean value between clockwise and counter-

clockwise rotation measured rate in tests exactly correspond to the value of vertical earth rotation rare projection (12.466 °/hour). In the cycles shown in Figure 11 the duration of rotation at current angular rate was 130 seconds (Fig. 12 left), which is relatively small time for such a slow rates accurate assessment. With increased duration of rotations (up to 900s – Fig. 12 right), the dispersion of output signal was decreased to its intrinsic minimum that corresponds to gyro instability. This limit corresponds to RMS = 1.4 ppm SF stability ( $\tau=900s$ ), compared with RMS = 3.5 ppm SF stability ( $\tau=130s$ ).

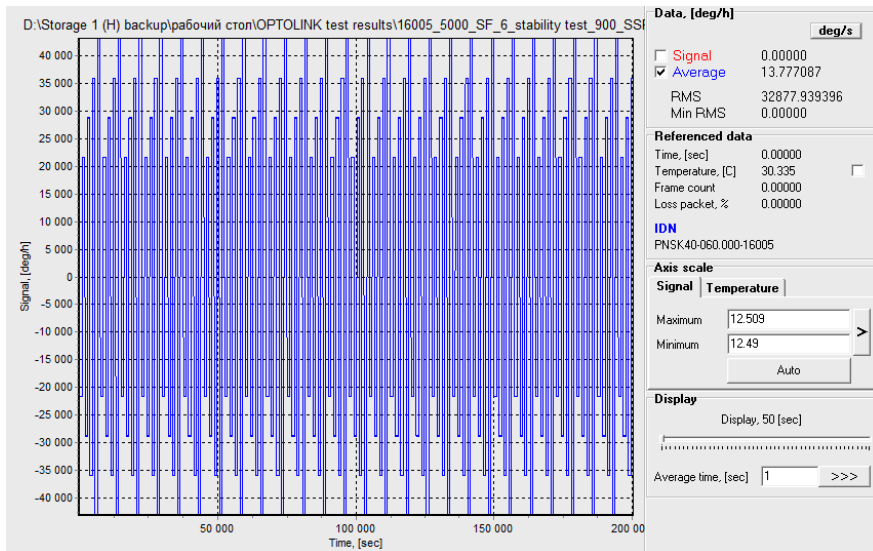


Figure 11. SRS-5000 №16005 Scale factor stability tests – raw data

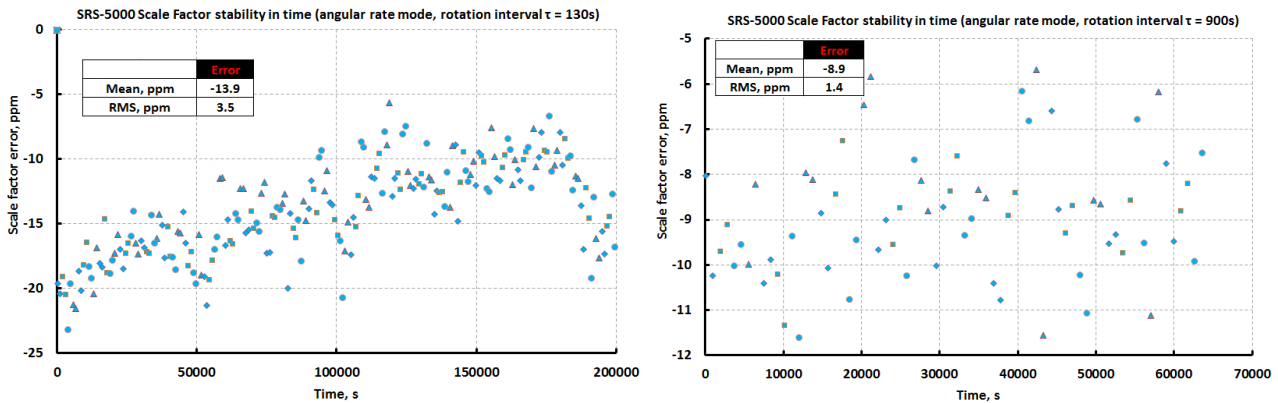


Figure 12. Scale factor stability test results. Duration of single rotation: 130s (left), 900s (right)

In general, Optolink uses angular rate basis for produced FOGs SF tests. Drawback is that this methodic relies on the repeatability and accuracy of rotation tables used, thus one needs to use expensive equipment, but plus is that data frame loss issues do not affect the estimation process. For SRS-5000 tests we used Acutronic AC2267-TC and Acutronic AC2247-TC 2-axis tables and single-axis rotation tables of our own manufacturing based

on Kollmorgen rotation mechanisms and control units. In addition to standard angular rate checks, which correspond to Figures 11-12, for SRS-5000 SF tests we also used the accumulated angle data output mode of gyro, and estimated SF error in angle basis. In this methodic one does not require precise rotation rate control, but requires high accuracy for table plate angular position estimation. In the setup used the angular tolerances were less than  $0.0005^\circ$ , enabling us to effectively estimate the SF value without introducing significant angle measurement error (error < 0.19 ppm). The procedure of tests was just the same, but in each step the final position of rotation table was secured and recorded into the data chart. Graphs of raw data and results of SF estimation according to this methodic are shown in Figure 13.

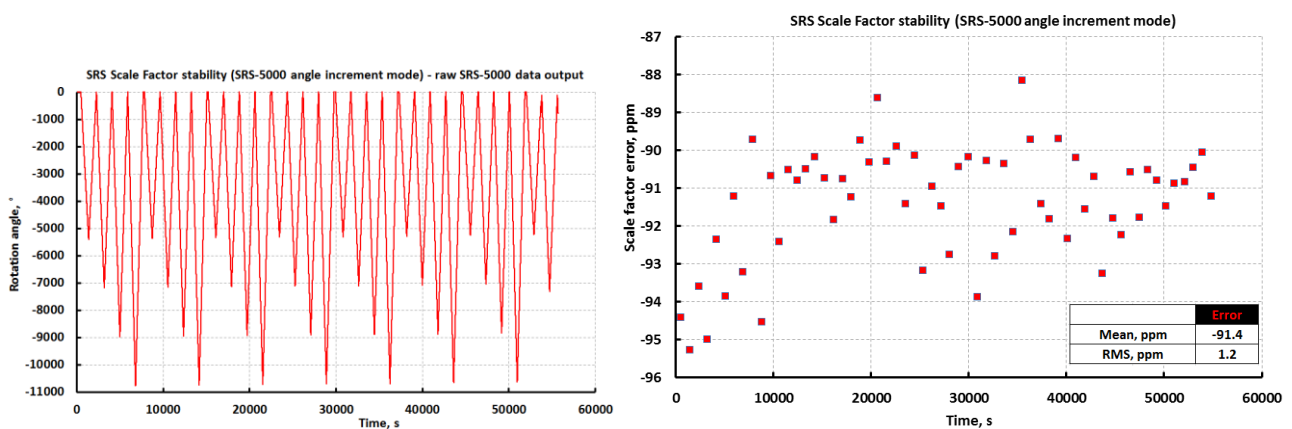


Figure 13. Scale factor stability raw data (left) and test results (right) in gyro angle increment mode

Despite the same overall RMS in tests that resulted 1.2 ppm and proved the value of SF stability of gyro in single launch, the additional error of -80 ppm was noticed. This error is due to the following fact, which has both pros and cons. The advantage is that while we measure the angle increment in the launch with gyro itself, it provides us robustness for data frame losses as the angular rate data of a damaged/lost frame is always included into the following frame sent by gyro. However, the disadvantage is that when gyro obtains the angle increment itself it integrated initial angular rate data over time, thus introducing the timing frequency error of internal clock into the output angle and into the effective SF estimation. In our tests -80 ppm error accounts for intrinsic clock frequency error of a gyro, and this was further justified with oscilloscope.

#### 4.5. SF repeatability (run-to-run) tests and SF long-term stability results

In addition to SF stability in single launch test we conducted SF repeatability (run-to-run) test of SRS-5000 gyros. The procedure was just the same as for bias run-to-run stability

test and SF single-launch stability tests, each reboot followed the cycle of clockwise and counter-clockwise rotations at a certain angular rate. In Figure 14 periodic green spikes towards  $-273\text{ }^{\circ}\text{C}$  (temperature of gyro) can be used as a sign of device reboot.

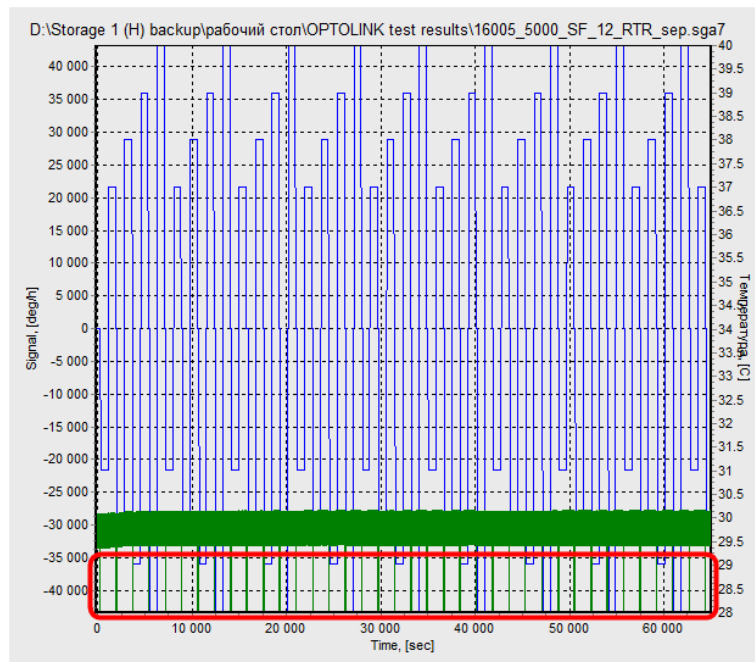


Figure 14. Scale factor run-to-run stability tests: raw data

Figure 15 (left) shows the results of run-to-run tests. The resulting SF RMS value in launches sequence was only a little higher than single-launch error: 2.5-2.8 ppm RMS compared to 1.2-1.4 ppm RMS, which indicates very good SF repeatability in short-term tests.

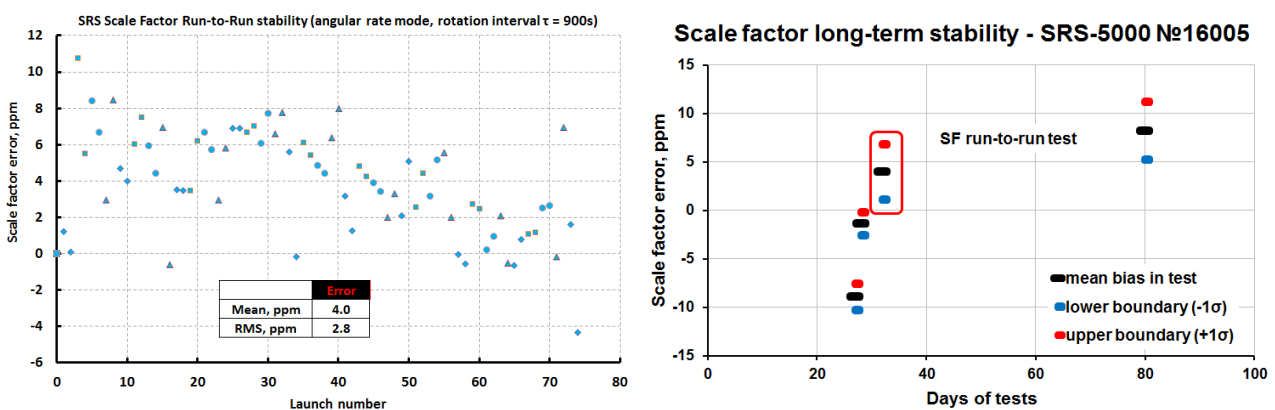


Figure 15. SRS-5000 №16005 SF test results: left - run-to-run stability; right - long-term stability

In addition, over large time period along with bias long-term stability we measured scale factor long-term stability. Graph representing the gyro SF drift in time are presented in Figure 15 (right). It has to mentioned, the values of SF error over 2-months usage were

within  $\pm 10$  ppm tolerance from zero value, which is the best result obtained for Optolink's gyroscopes so far.

#### 4.6. SRS-5000 gyro overall measurement results

Table 3 shows the evaluated and presented measurement results.

**Table 3. Evaluated values of FOG SRS-5000 performance characteristics**

Parameter	Value
<b>*Maximal absolute value of measured angular rate, °/s</b>	<b>*<math>\pm 12</math> (<math>\pm 550</math>)</b>
Scale factor error at constant temperature, ppm	$\leq 10$
Scale factor repeatability at constant temperature ( $1\sigma$ ), ppm	$\leq 3$
Angle random walk (according to Allan variance plot), $\mu^\circ/\sqrt{\text{hour}}$	$< 70$
Bias instability (according to Allan variance plot), $^\circ/\text{hour}$	$\leq 8 \times 10^{-5}$

**\*Dynamic range can be extended via scheme reported for SRS-1000 at ISS2014 [21].**

From the obtained results we can conclude SRS-5000 gyro type reaches strategic-grade performance ranges and can be considered as one of the most precise gyros available for purchase on the market.

#### 5. IMU-5000 and SINS-5000 on the basis of SRS-5000 gyro

Moreover, we have also produced pilot series of IMU and SINS (Strapdown Inertial Navigation Systems) on the basis of SRS-5000 FOG – SINS-5000. Pilot units of SINS-5000 are now under studying with estimated alignment accuracy limit down to RMS  $0.005^\circ$  in series of 9-minute alignments. Exterior of IMU-5000 block is shown in Figure 16.

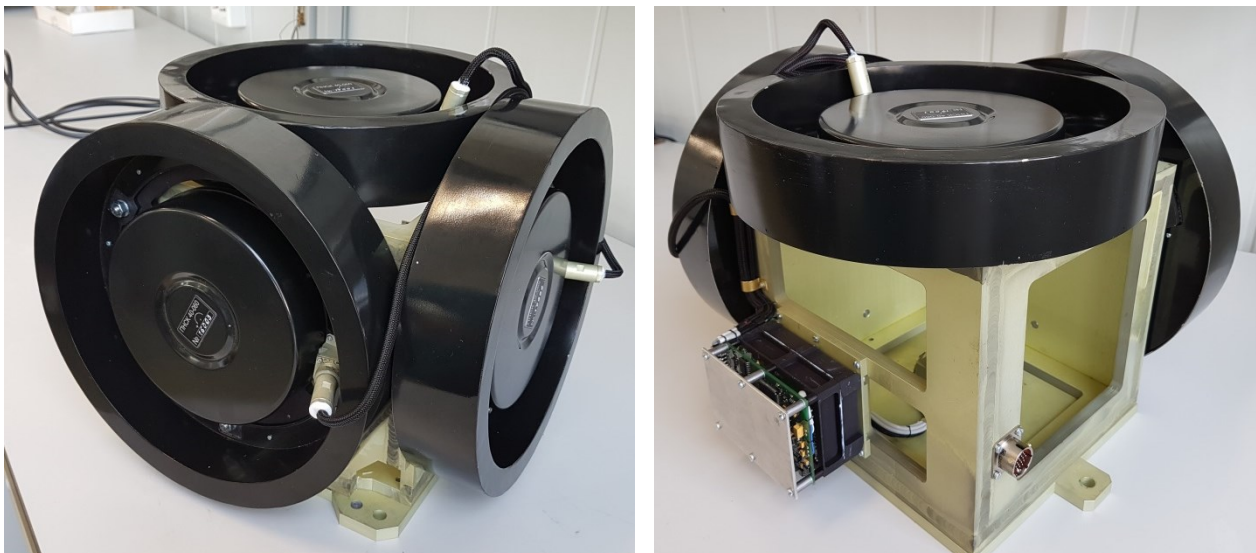


Figure 16. Exterior of IMU-5000 on the basis of SRS-5000

## 5. Conclusion

The aim of the current work was to produce the highest bias stability fiber-optic gyroscope SRS-5000. The Allan variance analysis of SRS-5000 FOGs shows that the ARW was around  $69 \mu^\circ/\sqrt{\text{hour}}$  with a bias stability of better than  $8 \times 10^{-5} \text{ }^\circ/\text{hour}$ . This bias performance, amongst the best closed loop fiber-optic gyroscope performance published to date, is equivalent to drift rate of less than one revolution per 5 centuries! Similarly, the SRS-5000 FOG bias instability and angle white noise level compare favorably to the best-ever published data for a hemispherical resonator gyroscope. Hence, we believe the noise and bias performance of this strategic-grade FOG may be useful in a range of high precision navigation, metrology, seismic, and structural sensing applications, as well as calibration of inertial test equipment.

## References

- [1] H. C. Lefèvre. Ultimate-performance fiber-optic gyroscope: A reality // In 16th Opto-Electronics and Communications Conference (OECC), Kaohsiung, Taiwan, (Jul. 2011), pp. 75-78.
- [2] H. C. Lefèvre. The fiber-optic gyroscope: Achievement and perspective // Gyroscopy and Navigation, 2012, Vol.3, pp.223-226.
- [3] H. C. Lefèvre. The fiber-optic gyroscope: Challenges to become the ultimate rotation-sensing technology // Optical Fiber Technology, 2013, 19 (6), pp.828-832.
- [4] G.A. Sanders, B. Szafraniec, L. Strandjord, R. Bergh, A. Kaliszek, R. Dankwort, D. Kimmel. Progress in high performance fiber optic gyroscopes // In Optical Fiber Sensors, Optical Society of America, 1997, p. OWB1.
- [5] S. Divakaruni, S. Sanders. Fiber optic gyros: a compelling choice for high precision applications // In Optical Fiber Sensors, Optical Society of America, 2006, p. MC2
- [6] S. Divakaruni, G. Keith, C. Narayanan, J. Keener // Strategic interferometric fiber-optic gyroscope for ballistic missile inertial guidance // AIAA Guidance, Navigation and Control Conference and Exhibit, 18 - 21 August 2008, Honolulu, paper 2008-7301.
- [7] S. Sanders, A. Taranta, S. Mosor, M. Alden, L. Hendry, R. DeMaio, N. Giere, J. Sewell. Fiber optic gyros in a high-performance, high-reliability inertial reference unit for commercial satellites // Proc. SPIE, 2012, vol.8421, OFS2012 22nd International Conference on Optical Fiber Sensors, pp.842106; doi: 10.1117/12.975535

- [8] [https://aerocontent.honeywell.com/aero/common/documents/Fiber\\_Optic\\_Gyro\\_Based\\_Inertial\\_Reference\\_System.pdf](https://aerocontent.honeywell.com/aero/common/documents/Fiber_Optic_Gyro_Based_Inertial_Reference_System.pdf)
- [9] K.M.Killian, M. Burmenko, W. Hollinger. High-performance fiber optic gyroscope with noise reduction // Proc. SPIE, 1994, vol.2292, Fiber Optic and Laser Sensors XII, pp. 255-263; doi: 10.1117/12.191838.
- [10] A. Cordova, R.A. Patterson, J. Rahn, L.K. Lam, D.M. Rozelle. Progress in navigation-grade IFOG performance // Proc. SPIE, 1996, vol.2837, Fiber Optic Gyros: 20th Anniversary Conference, pp. 207-217; doi: 10.1117/12.258181 .
- [11] <http://www2.l-3com.com/spacenav/pdf/datasheets/cirius-a.pdf>
- [12] [https://spaceequipment.airbusdefenceandspace.com/avionics/fiber-optic-gyroscopes/astrix-200/High-Performance\\_FOG\\_IMU](https://spaceequipment.airbusdefenceandspace.com/avionics/fiber-optic-gyroscopes/astrix-200/High-Performance_FOG_IMU)
- [13] Y. Paturel, V. Rumoroso, A. Chapelon, J. Honthaas. MARINS, the first FOG navigation system for submarines // In Symposium Gyro Technology, 2006, p. 17.
- [14] F. Guattari, C. Moluçon, A. Bigueur, E. Ducloux, E. de Toldi, J. Honthaas, H. Lefèvre. Touching the limit of FOG angular random walk: Challenges and applications // DGON Inertial Sensors and Systems (ISS) Proceedings, September 20-21, 2016, Karlsruhe, Germany, pp.1-13.
- [15] F. Bernauer, J. Wassermann, F. Guattari, H. Igel. Portable sensor technology for rotational ground motions // Geophysical Research Abstracts, 2016, Vol. 18, p. EGU2016-13345.
- [16] Y. N. Korkishko, V. A. Fedorov, V. E. Prilutskii, V. G. Ponomarev, V. G. Marchuk, I. V. Morev, E. M. Paderin, S. M. Kostritskii, V. N. Branets, V. S. Ryzhkov. Fiber optical gyroscope for space applications // in Optical Fiber Sensors, OSA Technical Digest (Optical Society of America, 2006), paper TuE91.
- [17] Yu.Korkishko, V.Fedorov, V.Prilutskii, V.Ponomarev, I.Morev, S. Kostritskii, A.Zuev, V.Varnakov. Closed loop fiber optical gyroscopes for commercial and space applications // in DGON Proc. Inertial Sensors and Systems - Symposium Gyro Technology 2012, Karlsruhe, Germany, 18-19 September 2012, pp.P14.1-P14.15.
- [18] Yu.N. Korkishko, V.A.Fedorov, V.E.Prilutskii, V.G.Ponomarev, I.V.Morev, S.M.Kostritskii. Interferometric closed-loop fiber-optic gyroscopes // Proc. SPIE, 2012, Vol.8351, Third Asia Pacific Optical Sensors Conference, 83513L.

- [19] Yu.N.Korkishko, V.A.Fedorov, V.E.Prilutskii, V.G.Ponomarev, I.V.Morev, S.M.Kostritskii, A.I.Zuev, V.K.Varnakov. Interferometric closed loop fiber optical gyroscopes for commercial and space applications // Proc.SPIE, 2012, vol.8421, OFS2012 22nd International Conference on Optical Fiber Sensors, 842107.
- [20] Yu.N.Korkishko, V.A.Fedorov, V.E.Prilutskiy, V.G.Ponomarev, I.V.Morev, D.V. Obuhovich, I.V.Fedorov, N.I.Krobka. Investigation and Identification of Noise Sources of High Precision Fiber Optic Gyroscopes// in Proc. 20th Saint Petersburg International Conference on Integrated Navigation Systems, Saint Petersburg, May 27-29, 2013, pp.59-62.
- [21] Yu.Korkishko, V.Fedorov, V.Prilutskii, V.Ponomarev, I.Morev, D. Obuhovich, S.Prilutskii. High-precision fiber optical gyro with extended dynamical range // in Proc. DGON Inertial Sensors and Systems - Symposium Gyro Technology 2014, Karlsruhe, Germany, 16-17 September 2014, pp.P09.1-P09.14.
- [22] Yu.N.Korkishko, V.A.Fedorov, V.E.Prilutskii, V.G.Ponomarev, I.V.Morev, S.F.Skripnikov, M.I.Khmelevskaya, A.S.Buravlev, S.M.Kostritskii, I.V.Fedorov, A.I.Zuev, V.K.Varnakov. Strapdown Inertial Navigation Systems Based on Fiber Optic Gyroscopes // Gyroscopy and Navigation, 2014, Vol. 4, No. 4, pp. 195–204.
- [23] Yu.N.Korkishko, V.A.Fedorov, V.E.Prilutskiy, V.G.Ponomarev, I.V.Morev, A.I.Morev, D.V.Obuhovich, S.M.Kostritskii, A.I.Zuev, V.K.Varnakov, A.V. Belashenko, E.N.Yakimov, G.V.Titov, A.V.Ovchinnikov, I.B.Abdul'minov, S.V.Latyntsev. Space grade fiber optic gyroscope: R&D results and flight tests // in Proc. 2016 DGON Inertial Sensors and Systems (ISS), Karlsruhe, Germany, 20-21 September 2016, p.21.1-21.19. [16] P. Lv, J. Liu, J. Lai, K. Huang. Allan variance method for gyro noise analysis using weighted least square algorithm // Optik-International Journal for Light and Electron Optics, 2015, 126(20), 2529.
- [24] D.J. Benford, D.J. Fixsen, S.A. Rinehart, M. Rizzo, S.F. Maher, R.K. Barry. Precision attitude control for the BETTII balloon-borne interferometer // Proc. SPIE, 2012, vol. 8444, Ground-based and Airborne Telescopes IV, 84442P; doi: 10.1117/12.927224;
- [25] M.J. Rizzo, S.A. Rinehart, J.B. Alcorn, R.B. Barclay, R.K Barry, D.J. Benford, A. Dhabal, D.J. Fixsen, A.S. Gore, S. Johnson-Shapoval, D.T. Leisawitz, S.F. Maher, L.G. Mundy, A. Papageorgiou, E. Pascale, A. Rau, R.F. Silverberg, P. Taraschi, T.J. Veach, S. Weinreich. Building an interferometer at the edge of space: pointing and

phase control system for BETTII // Proc. SPIE, 2014, vol. 9143, Space Telescopes and Instrumentation 2014: Optical, Infrared, and Millimeter Wave, 91433H;

- [26] S.A. Rinehart, M.J. Rizzo, D.J. Benford, D.J. Fixsen, T.J. Veach, A. Dhabal, J.G. Staguhn. The balloon experimental twin telescope for infrared interferometry (BETTII): an experiment for high angular resolution in the far-infrared // Publications of the Astronomical Society of the Pacific, 2014, 126(941), 660.
- [27] M.J. Rizzo, S.A. Rinehart, A. Dhabal, P. Ade, D. J. Benford, D. J. Fixsen, M. Griffin, R. Juanola-Parramon, D. T. Leisawitz, S. F. Maher, E. Mentzell, L. G. Mundy, A. Papageorgiou, E. Pascale, R. F. Silverberg, G. Savini, J. Staguhn, T. J. Veach, J. Vila Hernandez de Lorenzo. The Balloon Experimental Twin Telescope for Infrared Interferometry (BETTII): towards the first flight // Proc. SPIE, 2016, vol.9908, Ground-based and Airborne Instrumentation for Astronomy VI, 99080S;
- [28] M. Tajmar. Evaluation of enhanced frame-dragging in the vicinity of a rotating niobium superconductor, liquid helium and a helium superfluid // Superconductor Science and Technology, 2011, 24(12), 125011.
- [29] M. Tajmar, F. Plesescu, B. Seifert. Anomalous fiber optic gyroscope signals observed above spinning rings at low temperature // J. Phys.: Conf. Ser., 2009, 150:032101.
- [30] M. Tajmar, F. Plesescu. Fiber-optic-gyroscope measurements close to rotating liquid helium // AIP Conf. Proc. , 2010, 1208, 220.
- [31] M. Tajmar, F. Plesescu, B. Seifert. Precision angular velocity response of a fiber-optic gyroscope using a piezo nano-rotation table // Meas. Sci. Technol., 2009, 20, 027002.
- [32] Z. Gao, Y. Zhang, G. Wang, W. Gao. Analysis and simulation for the thermal performance of the octupolar fiber coil // Optical Engineering, 2014, 53(1), 016114.
- [33] W. Ling, X. Li, Z. Xu, Z. Zhang, Y. Wei. Thermal effects of fiber sensing coils in different winding pattern considering both thermal gradient and thermal stress // Optics Communications, 2015, 356, 290.
- [34] W.K. Burns, Phase Error Bounds of Fiber Gyro with Polarisation – Holding Fiber // J. Lightwave Technology, 1986, 4, pp.8-14.
- [35] Optical gyros and their application. / ed. by D. Loukianov, R. Rodloff, H. Sorg, B. Stieler // AGARD Technical Report RTO-AG-339, NATO Research and Technology Organisation, 1999.